Kristen L. Zakian, PhD
Kanishka Sircar, MD
Hedvig Hricak, MD, PhD
Hui-Ni Chen, MS
Amita Shukla-Dave, PhD
Steven Eberhardt, MD
Manickam Muruganandham, PhD
Lanie Ebora, BS
Michael W. Kattan, PhD
Victor E. Reuter, MD
Peter T. Scardino, MD
Jason A. Koutcher, MD, PhD

Published online
10.1148/radiol.2343040363
Radiology 2005; 234:804–814

Abbreviations:
Cho = choline-containing compound
Cit = citrate
Cr = creatine/phosphocreatine

[1] From the Departments of Medical Physics (K.L.Z., A.S.D., M.M., J.A.K.), Radiology (K.L.Z., H.H., H.N.C., A.S.D., S.E., L.E., J.A.K.), Pathology (K.S., V.E.R.), Urology (M.W.K., P.T.S.), Epidemiology and Biostatistics (M.W.K.), and Medicine (J.A.K.), Memorial Sloan-Kettering Cancer Center, 1275 York Ave, New York, NY 10021. From the 2002 RSNA Annual Meeting. Received February 24, 2004; revision requested April 7; revision received June 2; accepted July 1. Supported by National Institutes of Health grants R21 CA 84258-01 and 7-R01 CA76423. **Address correspondence to** K.L.Z. (e-mail: *zakiank@mskcc.org*).

Authors stated no financial relationship to disclose.

Author contributions:
Guarantor of integrity of entire study, K.L.Z.; study concepts, K.L.Z., H.H., J.A.K.; study design, K.L.Z., H.H., J.A.K., P.T.S.; literature research, K.L.Z., A.S.D.; clinical studies, K.L.Z., A.S.D., M.M., L.E., K.S., P.T.S., S.E., V.E.R.; data acquisition, A.S.D., M.M., K.S.; data analysis/interpretation, K.L.Z., S.E., A.S.D., L.E., H.C., M.W.K., V.E.R.; statistical analysis, H.C., M.W.K.; manuscript preparation, K.L.Z.; manuscript definition of intellectual content, K.L.Z., H.H., J.A.K.; manuscript editing, H.H., J.A.K., M.W.K.; manuscript revision/review and final version approval, all authors

Correlation of Proton MR Spectroscopic Imaging with Gleason Score Based on Step-Section Pathologic Analysis after Radical Prostatectomy[1]

PURPOSE: To determine whether hydrogen 1 magnetic resonance (MR) spectroscopic imaging can be used to predict aggressiveness of prostate cancer.

MATERIALS AND METHODS: All patients gave informed consent according to an institutionally approved research protocol. A total of 123 patients (median age, 58 years; age range, 40–74 years) who underwent endorectal MR imaging and MR spectroscopic imaging between January 2000 and December 2002 were included. MR imaging and spectroscopy were performed by using combined pelvic phased-array and endorectal probe. Water and lipids were suppressed, and phase-encoded data were acquired with 6.2-mm resolution. Voxels in the peripheral zone were considered suspicious for cancer if (Cho + Cr)/Cit was at least two standard deviations above the normal level, where Cho represents choline-containing compounds, Cr represents creatine and phosphocreatine, and Cit represents citrate. Correlation between metabolite ratio and four Gleason score groups identified at step-section pathologic evaluation (3 + 3, 3 + 4, 4 + 3, and ≥4 + 4) was assessed with generalized estimating equations.

RESULTS: Data from 94 patients were included. Pathologic evaluation was used to identify 239 lesions. Overall sensitivity of MR spectroscopic imaging was 56% for tumor detection, increasing from 44% in lesions with Gleason score of 3 + 3 to 89% in lesions with Gleason score greater than or equal to 4 + 4. There was a trend toward increasing (Cho + Cr)/Cit with increasing Gleason score in lesions identified correctly with MR spectroscopic imaging. Tumor volume assessed with MR spectroscopic imaging increased with increasing Gleason score.

CONCLUSION: MR spectroscopic imaging measurement of prostate tumor (Cho + Cr)/Cit and tumor volume correlate with pathologic Gleason score. There is overlap between MR spectroscopic imaging parameters at various Gleason score levels, which may reflect methodologic and physiologic variations. MR spectroscopic imaging has potential in noninvasive assessment of prostate cancer aggressiveness.

In patients with prostate cancer, the Gleason scores at biopsy (1–4) and at postsurgical pathologic evaluation (5–7) are important factors in predicting outcome, regardless of therapy. Biopsy Gleason score, while valuable, is subject to sampling error due to the finite number of cores that can be obtained. Furthermore, prostate cancer is histologically heterogeneous and is multifocal in most patients. It has been reported that the biopsy Gleason score is upgraded in as many as 54% of patients after radical prostatectomy (8). Thus, a noninvasive technique that could be used to assess prostate cancer aggressiveness and accurately predict the pathologic Gleason score could make a substantial contribution to the decision-making process in patients with prostate cancer.

Magnetic resonance (MR) spectroscopic imaging permits analysis of metabolism in the entire prostate gland. Combined with MR imaging, proton MR spectroscopic imaging has shown promise in helping in the detection of cancer in the prostate peripheral zone (9). The goal of the current study was to determine whether metabolic information provided by MR spectroscopic imaging could be used to predict the aggressiveness of prostate cancer.

TABLE 1
Clinical Data for Study Patients

Characteristic	Value
Median age (y)	58.20 (40–74)*
Median prostate-specific antigen level (ng/mL)	5.8 (1.06–72.00)*
Clinical stage	
T1b	1 (0.8)
T1c	61 (49.6)
T2a	39 (31.7)
T2b	14 (11.4)
T2c	7 (5.7)
T3a	1 (0.8)
Biopsy Gleason score	
3 + 2	1 (0.8)
3 + 3	65 (52.8)
3 + 4	38 (30.9)
4 + 3	5 (4.1)
4 + 4	9 (7.3)
4 + 5	5 (4.1)

Note.—Unless otherwise indicated, data are number of patients, and data in parentheses are percentages.
* Data in parentheses are the range.

MATERIALS AND METHODS

Patient Demographics

A total of 123 patients (median age, 58 years; age range, 40–74 years) who underwent endorectal MR imaging and hydrogen 1 MR spectroscopic imaging followed by radical prostatectomy between January 2000 and December 2002 were included in this study. All patients gave informed consent according to an institutionally approved research protocol. The clinical information for these patients is shown in Table 1. A minimum delay of 6 weeks was required between biopsy and MR imaging and MR spectroscopic imaging to minimize biopsy artifacts. Patients whose surgery was more than 6 months after MR imaging and MR spectroscopic imaging were not included in the study. The average time elapsed between the combined MR imaging and spectroscopic imaging examination and radical prostatectomy was 41.7 days ± 34.5 (mean ± standard deviation). Following surgery, radical prostatectomy specimens were submitted for whole-mount step-section pathologic evaluation.

Data Acquisition

MR imaging and MR spectroscopic imaging were performed with a 1.5-T Signa Horizon MR system (GE Medical Systems, Milwaukee, Wis) that used MR spectroscopic imaging software developed at the University of California at San Francisco (10–14). In the imaging portion of the study, T1-weighted transverse images were obtained from the aortic bifurcation to approximately 1 cm inferior to the distal prostatic apex by using a spin-echo pulse sequence (repetition time msec/echo time msec, 700/14; field of view, 24 cm; section thickness, 5 mm; section gap, 1 mm; number of acquisitions, two). T2-weighted images in the transverse and coronal planes were acquired by using a fast spin-echo sequence (4000/102; echo train length, 12; field of view, 14 cm; section thickness, 3 mm; no section gap; number of acquisitions, four). Spectroscopic imaging consisted of point-resolved spectroscopy voxel excitation (15) with band-selective inversion with gradient dephasing water and lipid suppression (11). Chemical shift imaging (16) with a matrix of either $16 \times 8 \times 8$ or $8 \times 8 \times 8$ was performed over fields of view of $100 \times 50 \times 50$ mm or $50 \times 50 \times 50$ mm, which resulted in spatial resolution of 6.25 mm in all three dimensions. One or two signals were acquired depending on the number of spatial encodes, which yielded an imaging time of 17 minutes. The entire MR imaging and MR spectroscopic imaging examination required approximately 1 hour.

Spectroscopic Data Processing

Data processing was performed at an Ultra 10 workstation (Sun Microsystems, Mountain View, Calif) and included 2-Hz Lorentzian spectral apodization, four-dimensional Fourier transformation, and automated frequency, phase, and baseline correction (14). While data were acquired with 6.2-mm spatial resolution, interpolation in the superior-inferior dimension gave an effective voxel size of 0.12 cm^3 for data analysis. Peak areas were calculated with numeric integration. The standard deviation of noise over a frequency range equivalent to the peak integration range but in an area containing only noise was calculated for each peak to provide a noise measure. The peak areas were then normalized with respect to the standard deviation of noise to give an approximate signal-to-noise ratio. Each voxel was classified as healthy, suspicious for cancer, very suspicious for cancer, or having nondiagnostic levels of metabolites or artifact that obscured the metabolite frequency range (K.L.Z., 5 years of experience with prostate spectroscopy). Voxels were considered suspicious for cancer if the ratio of choline-containing compounds (Cho) and creatine/phosphocreatine (Cr) to citrate (Cit) (ie, [Cho + Cr]/Cit) was at least 2 standard deviations above the average healthy ratio for the peripheral zone as reported by Males et al (17). Voxels were considered to be very suspicious for cancer if (Cho + Cr)/Cit was more than three standard deviations above the average healthy ratio. Voxels considered to be nondiagnostic contained no metabolites with a signal-to-noise ratio greater than five. In voxels where only one metabolite was detectable, the other metabolites were assigned a value equivalent to the standard deviation of noise. For all voxels considered suspicious or very suspicious, (Cho + Cr)/Cit was recorded for statistical analysis. Only voxels in the peripheral zone were considered in this analysis. The MR spectroscopic imaging assignment of suspicious voxels was performed by using only (Cho + Cr)/Cit and without reference to the MR imaging findings or knowledge of the results of pathologic evaluation.

Pathologic Evaluation

Prostatectomy specimen whole-mount preparation consisted of surface inking

with tattoo dye (green dye was used on the right side of the specimen, and blue dye was used on the left) and was followed by fixation in 10% formalin for 36 hours. The distal 5-mm portion of the apex was amputated and coned. The remainder of the gland was serially sliced from the apex to the base at 3–4 mm intervals, and slices were submitted for paraffin embedding as whole mounts. The seminal vesicles were amputated and submitted separately. After paraffin embedding, microslices were placed on glass slides and stained with hematoxylin and eosin. At pathologic analysis, a Gleason score was assigned to the whole cancer in the specimen according to the current clinical protocol at our institution. In addition, cancer foci were outlined in ink on whole-mount, apical, and seminal vesicle slices, so as to be grossly visible, and then photographed (K.S., 3 years experience). These constituted the tumor maps. Components of the tumor region in lesions with a Gleason score of 3 or greater than or equal to 4 were outlined in green and black, respectively, so that the proportion of each Gleason pattern could be assessed in individual lesions, and each lesion was assigned a Gleason score (3 + 3, 3 + 4, 4 + 3, or ≥4 + 4). Lesions with a Gleason score greater than or equal to 4 + 4 were grouped into one category. The largest in-plane diameter of each lesion at step-section pathologic evaluation was also recorded.

MR Spectroscopic Imaging and Pathologic Evaluation Correlation

A radiologist (S.E., 4 years experience) matched the whole-mount pathologic step-section slices with the most closely corresponding T2-weighted MR images. Because resection and fixation can result in deformation of the gland and because of the impossibility of sectioning identical planes with the two techniques, exact correspondence between pathologic slices and MR sections was not expected. The most closely corresponding transverse T2-weighted images and pathologic step-section slices were paired on the basis of the following anatomic landmarks: *(a)* the presence of urinary bladder and seminal vesicle tissue in superior slices, *(b)* the slice with the largest diameter and progressive changes in the diameter of the slices, *(c)* the slice where the ejaculatory ducts enter the verumontanum, *(d)* the anterior-posterior and left-right position of the ejaculatory ducts and urethra and the shape of the urethra, *(e)* the thickness of the peripheral zone and the position of the pseudocapsule, and *(f)* the presence, size, and shape of the transition zone. The precision of matching in the superior-inferior direction was estimated as being within one transverse slice (±3 mm).

Because the MR spectroscopic data were acquired with the patient in the same position and with the same gradients as were used to acquire the MR imaging data, registration of the spectroscopic data with the T2-weighted images was automatic, and the spectroscopic data could then be compared with the most closely corresponding pathologic step-section data. For each lesion identified with pathologic evaluation, it was determined whether the lesion was detected with spectroscopy. The lesion was considered to have been detected with spectroscopy if at least one voxel had been categorized as suspicious or very suspicious for cancer in the corresponding sextant, anteroposterior position, and within one slice of the most closely corresponding pathologic section. These criteria reflect the limit to which lesions detected with MR spectroscopic imaging and those detected with pathologic evaluation can be matched accurately because of the factors described previously. When the lesion was detected with spectroscopy, it was designated as true-positive, and the (Cho + Cr)/Cit value for each suspicious voxel within the lesion was tabulated. The mean and maximum values of (Cho + Cr)/Cit for each lesion and the total number of suspicious voxels in the lesion were recorded for statistical analysis. The total number of suspicious voxels at MR spectroscopic imaging provided a surrogate for MR spectroscopic imaging tumor volume. All sites where MR spectroscopic imaging indicated a false-positive cancer and all sites where pathologic evaluation indicated a tumor but MR spectroscopic imaging did not depict it (false-negative cases) were also recorded. The (Cho + Cr)/Cit values in false-positive regions were tabulated.

Data and Statistical Analysis

Gleason scores at biopsy (maximum) and surgery (whole gland) were compared, and the number of patients whose scores at surgery remained the same, increased, or decreased were calculated. The MR spectroscopic imaging analysis was divided into two parts. In the first part of analysis, MR spectroscopic imaging sensitivity and specificity for cancer detection were analyzed prospectively by comparing the MR spectroscopic imaging voxels, which had been designated as suspicious or very suspicious for cancer, with the pathologic findings. Sensitivity was calculated for all pathologic lesions as a group and for individual Gleason score groups (3 + 3, 3 + 4, 4 + 3, and ≥4 + 4). For lesions with a Gleason score of 3 + 3, the influence of lesion size on detection sensitivity was assessed by calculating the average diameter of the true-positive lesions and false-negative lesions, as measured on the pathologic specimens.

The second part of the MR spectroscopic imaging analysis tested the hypothesis that MR spectroscopic imaging metabolite ratios in true-positive lesions were related to pathologic Gleason scores. Because the Gleason scores for the individual lesions and the whole gland were available, the relationship of both of these parameters to the MR spectroscopic imaging (Cho + Cr)/Cit value was assessed. Analysis of individual true-positive lesions was performed. For a given true-positive lesion, two indexes were chosen to represent the metabolic status: The first index chosen was the mean value of (Cho + Cr)/Cit over all voxels in the lesion. The second index was the maximum value of (Cho + Cr)/Cit in any voxel in the lesion. Both of these values were tested to determine whether one allowed better discrimination between lesion Gleason scores.

In each lesion, the MR spectroscopic imaging mean or maximum ratio was compared with the Gleason score for that lesion. The ability to discriminate between four lesion score groups (3 + 3, 3 + 4, 4 + 3, and ≥4 + 4) on the basis of the (Cho + Cr)/Cit ratio was assessed by using the generalized estimating equations technique (18), which is an extension of generalized linear models that provide a semiparametric approach to clusters of correlated measurements. This method accounts for the correlated measurements that arise when multiple lesions are found in the same patient. The natural logarithm of the metabolite ratio was used for analysis because the distribution was skewed to the right. In this analysis, the dependent variable was the MR spectroscopic imaging index, and the independent variable was the lesion Gleason score. The Gleason 7 subcategories were analyzed as separate groups because there may be a clinical benefit in distinguishing Gleason 3 + 4 and 4 + 3 cancers. Because the nominal resolution of the MR spectroscopic imaging study was 6.2 mm, it was expected that assessing aggressiveness in lesions smaller than the MR spectroscopic imaging voxel size would be less

TABLE 2
Patient Gleason Scores at Biopsy and at Radical Prostatectomy

	Radical Prostatectomy Gleason Score						
Biopsy Gleason Score	3 + 2	3 + 3	3 + 4	4 + 3	4 + 4	4 + 5	5 + 4
3 + 2	0	1*	0	0	0	0	0
3 + 3	0	50	14*	1*	0	0	0
3 + 4	0	5†	22	10*	1*	0	0
4 + 3	0	1†	1†	2	1*	0	0
4 + 4	0	0	2†	1†	3	2*	1*
4 + 5	0	0	1†	0	0	2	2*
5 + 4	0	0	0	0	0	0	0

* Gleason score was upgraded after surgery.
† Gleason score was downgraded after surgery.

accurate. Thus, the previously mentioned analysis was also performed with lesions segregated into groups. The first group consisted of lesions with maximum in-plane diameter of 5 mm or smaller at step-section pathologic evaluation, and the second group consisted of lesions with a maximum diameter larger than 5 mm.

To determine whether MR spectroscopic imaging metabolite ratios could be related to the pathologic whole-gland Gleason score, we attempted to create analogous metabolic indexes that incorporated metabolite ratios from all true-positive MR spectroscopic imaging lesions in the peripheral zone. Two indexes were calculated: the average (Cho + Cr)/Cit value for all true-positive suspicious voxels in the gland and the average of the individual true-positive lesion maximum (Cho + Cr)/Cit values. The effectiveness of each of these parameters in discrimination between four whole-gland Gleason score groups (3 + 3, 3 + 4, 4 + 3, and ≥4 + 4) was assessed by using analysis of variance; the MR spectroscopic imaging index served as the dependent variable, and the gland Gleason score served as the independent variable. The generalized estimating equations technique was not used because each test used only a single MR spectroscopic imaging index from each patient.

On the basis of information in the literature and a qualitative examination of MR spectroscopic tumor volume data, it was expected that a correlation could exist between tumor volume data and Gleason score. To determine whether a relationship existed between tumor volume data and Gleason score in the present study, generalized estimating equations were used to compare two indexes related to tumor volume with the lesion Gleason score. These indexes were the largest in-plane diameter measured in the step section and the number of suspicious MR spectroscopic imaging voxels composing the lesion (ie, MR spectroscopic imaging tumor volume). In these analyses, the tumor volume index was the dependent variable, and the lesion Gleason score was the independent variable.

Finally, receiver operating characteristic curve analysis was performed to determine whether adding tumor volume information to metabolite ratio data improved the ability to predict whether a tumor was low or high grade. For the purposes of this analysis, lesions with a Gleason score of 3 + 3 or 3 + 4 were classified as low-grade lesions, and lesions with a Gleason score of 4 + 3 or greater than or equal to 4 + 4 were classified as high-grade lesions. In a binary logistic regression model, the MR spectroscopic imaging tumor volume and the lesion maximum (Cho + Cr)/Cit data were considered as two separate predictors, and high- or low-grade cancer was the outcome variable. The goodness of fit of this model was assessed with the Hosmer-Lemeshow test. The predicted probabilities of the model were then used to construct the receiver operating characteristic curve. The area under the receiver operating characteristic curve was estimated by using the bootstrapping technique with 200 resamples to calculate an unbiased measure of the ability to discriminate high- and low-grade cancer.

In all statistical methods, a *P* value of less than .05 was considered to indicate a significant difference. All statistical analyses were conducted with the S-Plus 2000 Professional (Insightful, Seattle, Wash) and SAS 8.2 (SAS Institute, Cary, NC) software packages.

RESULTS

Patient Gleason Scores

Gleason scores at biopsy and whole-gland surgical-pathologic evaluation are shown in Table 2. At pathologic evaluation, 33 patients (26.8%) were assigned a higher Gleason score than that assigned at biopsy, 11 (8.9%) were assigned a lower score, and 79 (64.2%) were assigned the same score. Thus, biopsy was used to predict the correct surgical Gleason score in 64.2% of patients.

MR Spectroscopic Imaging Sensitivity and Specificity

Of the 123 patients who underwent MR imaging and MR spectroscopic imaging followed by radical prostatectomy, 94 were included in the final analysis of spectroscopy data. Reasons for exclusion included hardware failure (3); unusable MR data due to biopsy artifact, lipid contamination, or poor signal-to-noise ratio (13); chronic prostatitis identified at surgical pathologic evaluation (8); tumor present only in the transition zone (4); and more than 6 months between MR imaging and MR spectroscopic imaging and surgery (1). In these 94 patients, a total of 239 peripheral zone lesions were identified with step-section pathologic evaluation. Of these lesions, 135 were detected with MR spectroscopic imaging. The sensitivity of MR spectroscopic imaging in the detection of tumors is reported for all 239 lesions as a group and for lesions segregated by Gleason score (Table 3).

The data indicate that sensitivity of MR spectroscopic imaging appears to improve with higher Gleason score, with a detection rate greater than 85% for tumors with a Gleason score of 4 + 3 or greater than or equal to 4 + 4. Among the tumors with a Gleason score of 3 + 3, in which sensitivity was 44.4%, it was found at pathologic evaluation that the average largest diameter of the lesions that were not detected with MR spectroscopic imaging was 7.9 mm ± 4.9, while the average largest diameter of the tu-

TABLE 3
MR Spectroscopic Imaging Detection Sensitivity for Peripheral Zone Tumors Identified with Step-Section Pathologic Analysis

MR Spectroscopic Imaging	Lesion Gleason Score				Total
	3 + 3	3 + 4	4 + 3	≥4 + 4	
Diagnosis					
True-positive	72	33	13	17	135
False-negative	90	10	2	2	104
Total	162	43	15	19	239
Sensitivity (%)	44.4 (72/162)	76.7 (33/43)	86.7 (13/15)	89.5 (17/19)	56.5 (135/239)

Note.—Data in parentheses were used to calculate sensitivity.

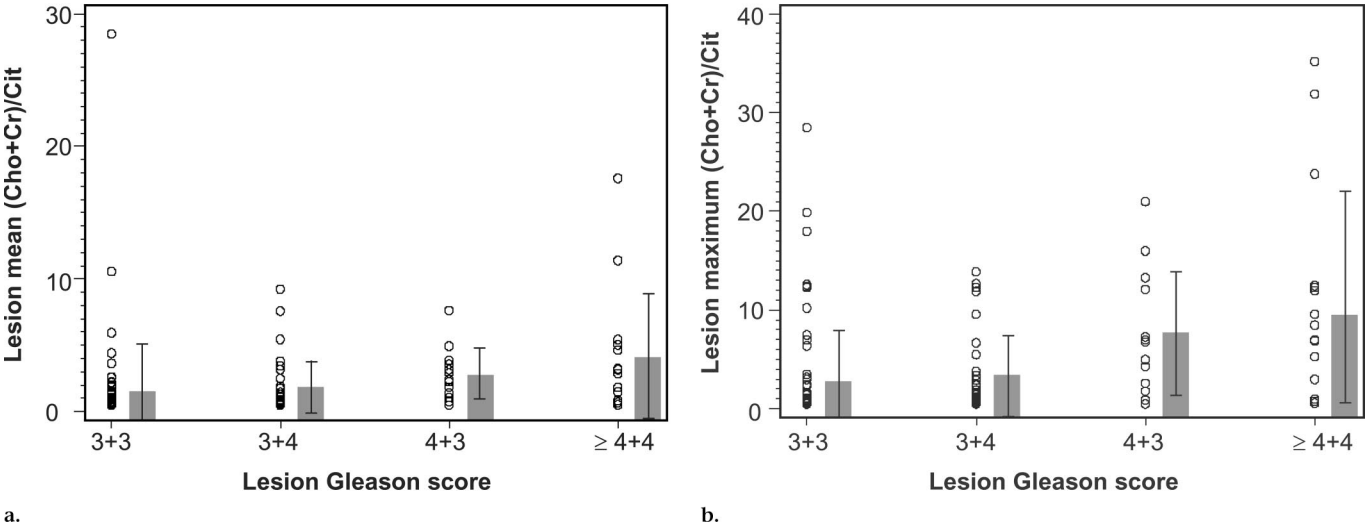

Figure 1. Graph shows **(a)** mean and **(b)** maximum MR spectroscopic imaging (Cho + Cr)/Cit value versus Gleason score in lesions. Gray columns represent mean value and error bars represent standard deviation of all lesions at that Gleason score. While there is a trend toward increasing ratio with increasing Gleason score, there is overlap between all groups.

mors that were detected with MR spectroscopic imaging was 11.6 mm ± 6.8 ($P <$ .001). MR spectroscopic imaging also indicated 127 false-positive voxels at 61 sites. The median (Cho + Cr)/Cit value from all the false-positive voxels was 0.7, and ratios were rounded off to the nearest tenth with the processing software. Approximately half of the false-positive voxels had (Cho + Cr)/Cit values that were between two and three standard deviations greater than the mean normal value; therefore, these voxels were considered suspicious but not very suspicious for cancer.

MR Spectroscopic Imaging Assessment of Tumor Aggressiveness

Of the 135 lesions correctly identified with MR spectroscopic imaging, 72 had a Gleason score of 3 + 3, 33 had a Gleason score of 3 + 4, 13 had a Gleason score of 4 + 3, and 17 had a Gleason score greater than or equal to 4 + 4. Both the mean (Cho + Cr)/Cit value and the maximum (Cho + Cr)/Cit value for each lesion increased with increasing lesion Gleason score (Fig 1). While this trend is clear, the error bars indicate that there is overlap between (Cho + Cr)/Cit values in all four of the Gleason score categories. The high outlying point in the Gleason 3 + 3 column in both graphs corresponds to a suspicious site that consisted of one voxel in which Cho was the sole detectable metabolite and Cit and Cr were assigned the noise value, as described in the Materials and Methods section. Representative data from healthy peripheral zones and glands with Gleason 3 + 3 and 4 + 4 cancers are shown in Figures 2–4. While a quantitative analysis of individual metabolite concentrations was not performed, these spectra indicate that the pattern of metabolites changes from one of slightly elevated Cho and moderate Cit levels in low-grade tumors to one of highly elevated Cho and low or absent Cit levels in high-grade tumors.

Tables 4 and 5 contain the *P* values for discriminating between Gleason scores in lesions on the basis of the (Cho + Cr)/Cit value. Both mean and maximum (Cho + Cr)/Cit values differed significantly in *(a)* lesions with a Gleason score of 3 + 3 versus those with a Gleason score of 4 + 3, *(b)* lesions with a Gleason score of 3 + 3 versus those with a Gleason score greater than or equal to 4 + 4, and *(c)* lesions with a Gleason score of 3 + 4 versus those with a Gleason score greater than or equal to 4 + 4. In addition, the mean ratio differed significantly in lesions with a Gleason score of 3 + 3 versus those with a Gleason score of 3 + 4, while the maximum ratio differed significantly in

lesions with a Gleason score of 3 + 4 versus those with a Gleason score of 4 + 3. In neither case did lesions with a Gleason score of 4 + 3 versus those with a Gleason score greater than or equal to 4 + 4 differ significantly from one another.

When lesions were segregated into those with an in-plane diameter of 5 mm or less at step-section pathologic evaluation versus those with a diameter of more than 5 mm, the small lesion group could not be analyzed with the generalized estimating equations technique because of the small number of lesions (n = 17). The group of lesions with a diameter larger than 5 mm showed trends similar to the unsegregated data, with substantial differences between lesions with the following Gleason scores in both the mean and maximum data: *(a)* lesions with a Gleason score of 3 + 3 versus those with a Gleason score of 4 + 3, *(b)* lesions with a Gleason score of 3 + 3 versus those with a Gleason score greater than or equal to 4 + 4, *(c)* lesions with a Gleason score of 3 + 4 versus those with a Gleason score greater than or equal to 4 + 3, and *(d)* lesions with a Gleason score of 3 + 4 versus those with a Gleason score greater than or equal to 4 + 4 (data not shown).

The results for the surgical (ie, whole-gland) Gleason score versus MR spectroscopic imaging data representing all true-positive voxels in the gland (Tables 6, 7) were similar to the individual lesion results. When the whole gland was represented by either the average of the individual lesion mean ratios or the average of the individual lesion maximum ratios, the following surgical-pathologic evaluation Gleason scores differed substantially *(a)* lesions with a Gleason score of 3 + 3 versus those with a Gleason score of 4 + 3, *(b)* lesions with a Gleason score of 3 + 3 versus those with a Gleason score greater than or equal to 4 + 4, *(c)* lesions with a Gleason score of 3 + 4 versus those with a Gleason score of 4 + 3, and *(d)* lesions with a Gleason score of 3 + 4 versus those with a Gleason score greater than or equal to 4 + 4.

Both the largest diameter on the pathologic slice and the number of voxels in the lesion (ie, MR spectroscopic imaging tumor volume) appeared to correlate positively with Gleason score. As was the case with the metabolite ratios, the MR spectroscopic imaging tumor volume showed overlap between all Gleason score groups (Fig 5). Receiver operating characteristics analysis of the ability to classify lesions as low or high grade gave a bootstrap-corrected area under the curve of 0.805 for MR spectroscopic imaging maximum ratio alone, 0.846 for MR spectroscopic imaging tumor volume alone, and 0.854 for MR spectroscopic imaging ratio and MR spectroscopic imaging tumor volume combined.

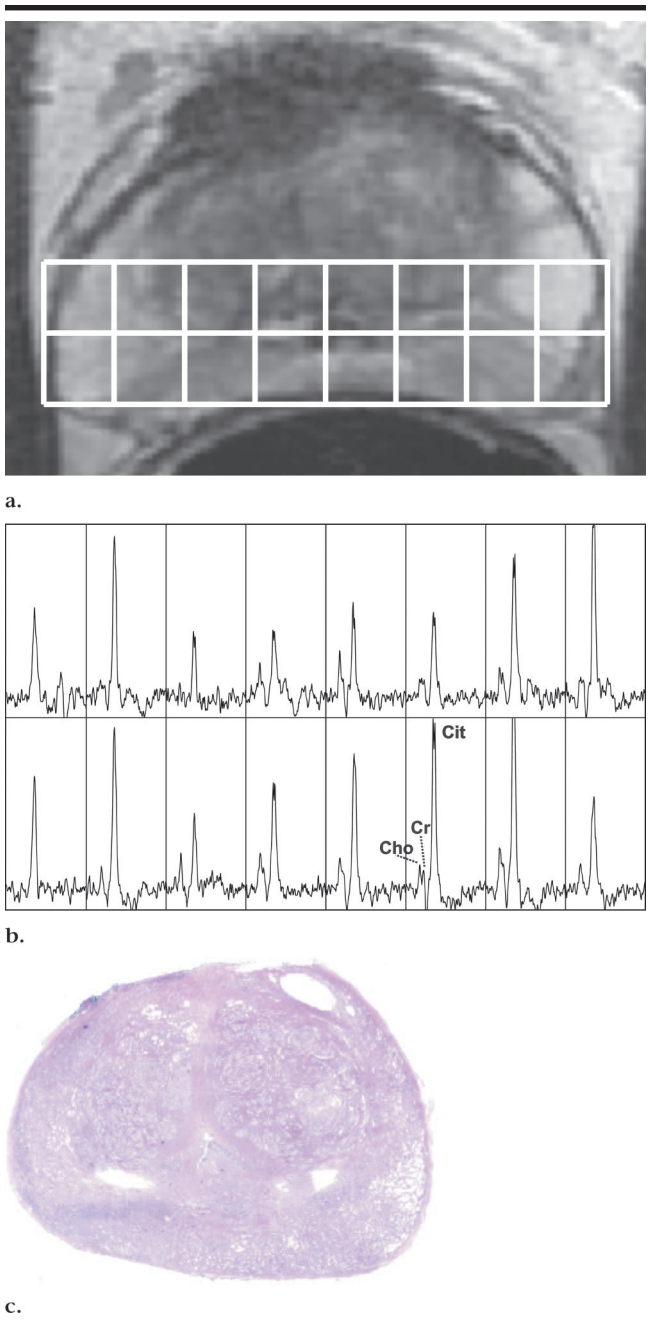

Figure 2. **(a)** Transverse T2-weighted MR image, **(b)** spectra corresponding to the grid in **a**, and **(c)** step-section pathologic tumor map for a healthy section of prostate gland show no cancerous areas. Transverse T2-weighted MR imaging parameters were as follows: 4000/102; echo-train length, 12; field of view, 14 cm; acquisition matrix, 256 × 192; section thickness, 3 mm; no section gap; number of acquisitions, three. MR spectroscopic imaging acquisition parameters were as follows: volume excitation with band-selective inversion with gradient dephasing water and lipid suppression; 1000/130; chemical shift imaging matrix, 16 × 8 × 8; field of view, 100 × 50 × 50 mm; spatial resolution, 6.25 mm; number of acquisitions, one; imaging time, 17 minutes.

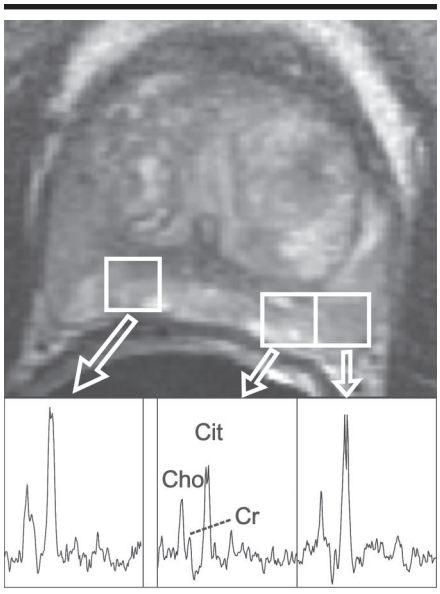

a.

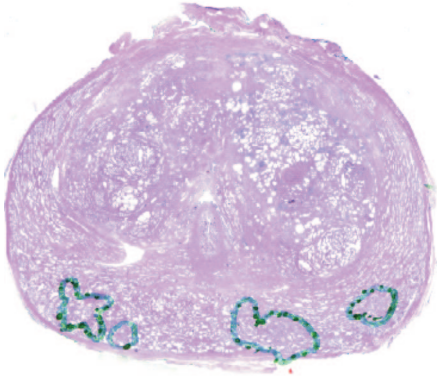

b.

Figure 3. **(a)** Transverse T2-weighted MR image with cancer voxels highlighted and corresponding spectra and **(b)** step-section pathologic tumor obtained in a patient with cancer with a Gleason score of 3 + 3 in the peripheral zone. Areas with a Gleason score of 3 + 3 are outlined. Cit is present in the tumor voxels, and the Cho level is moderately elevated. MR imaging and MR spectroscopy acquisition parameters are the same as those in Figure 2.

DISCUSSION

One of the most challenging characteristics of prostate cancer is its variable biologic aggressiveness. Usually classified at staging according to the biopsy Gleason score, prostate cancer aggressiveness is a key predictor of outcome. Prostate cancer is a multifocal and histologically heterogeneous disease, however, and biopsy is limited in the determination of all cancer sites and grades. In fact, when biopsy results were compared with radical prostatectomy for sextant tumor localization, the positive predictive value of biopsy was found to be 83.3%, and the negative predictive value was found to be 36.4% (19). Studies of 226 and 449 patients found that biopsy was used to correctly predict radical prostatectomy Gleason score in 31% and 58% of cases, respectively (8,20). Cookson et al (8) found that 54% of biopsies were undergraded and 15% were overgraded. In the present study, biopsy was used to correctly predict the pathologic Gleason score in 64% of patients; 27% were upgraded, and 9% were downgraded. Thus, there is room for improvement in the a priori determination of tumor aggressiveness, particularly if noninvasive assessment of the whole gland is possible.

Combined MR imaging and MR spectroscopic imaging aids in tumor localization within the peripheral zone (9,10,21), and preliminary reports of MR spectroscopic imaging assessment of tumor aggressiveness have shown promise (22,23). In the present study, in a larger number of patients and with step-section pathologic correlation, we have confirmed these preliminary results and extended them to show several important findings. First, we have confirmed that the ratio of Cho and Cr to Cit in the lesion is positively correlated with the lesion Gleason score, with elevation of Cho level and reduction of Cit level with increasing cancer aggressiveness. Second, the same result was found when either the lesion mean or maximum (Cho + Cr)/Cit value was assessed. In addition, when an overall mean or maximum (Cho + Cr)/Cit index was calculated for the gland, there was a positive correlation between that value and the surgical Gleason score. This latter finding is perhaps more clinically relevant, since the surgical Gleason score is used widely in models that are used to predict outcome. Finally, tumor volume measured with MR spectroscopic imaging also increased with increasing lesion Gleason score.

The Gleason scoring system is used to assign increasing pattern grades as the glands formed by the prostate epithelial cells become more poorly differentiated, the margins of the tumor become more poorly defined, and the degree of stromal invasion increases (24). Thus, there are several mechanisms by which Cit would be expected to decrease and Cho would be expected to increase with increasing Gleason grade.

Benign prostate epithelial cells produce high levels of Cit, probably as a result of the suppression of aconitase, which catalyzes the oxidation of Cit in the Krebs cycle (25). With dedifferentiation of normal epithelial cells, the ability to generate and concentrate Cit is expected to be lost. Architecturally, as normal glandular structure is lost, the high extracellular volume of Cit found in normal glands decreases. Thus, one might expect that with dedifferentiation, the Cit concentration would decrease.

Numerous investigators have found elevated Cho levels in tumors (26–32). Since these compounds are anabolites (choline and phosphocholine) and catabolites (glycerophosphocholine) of phosphatidylcholine, which is a major membrane phospholipid, it has been suggested that the elevated Cho peak reflects an elevated cell proliferation rate, and there are some data to support this hypothesis (33). It has also been reported, however, that cells in culture with similar proliferation rates have different Cho profiles; specifically, phosphocholine, glycerophosphocholine, and total choline increased as cells progressed from benign to malignant phenotypes (34). It was suggested that up-regulation of enzymes in the phosphatidylcholine pathway in more malignant tumors could explain the increased total choline levels. While much valuable work has been done, more research is required to fully elucidate the reasons for the elevation in Cho level in tumors and the apparent correlation of Cho level with aggressiveness.

A corollary to the finding that the (Cho + Cr)/Cit value increases with increasing Gleason score is that the sensitivity of MR spectroscopic imaging for cancer detection depends on the grade. In cancer with a Gleason score of 3 + 3, MR spectroscopic imaging tumor detection sensitivity was 44.4%, and sensitivity increased to 89.5% in cancers with a Gleason score of more than 8. Thus, a large proportion of tumors with a Gleason score of 6 did not generate abnormal voxel metabolite ratios. One possible explanation for this finding is that these tumors tended to be smaller, thus permitting volume averaging with noncancerous tissue. In fact, tumors with a Gleason score of 6 that were not detected with MR spectroscopic imaging had significantly smaller average diameters than those that were detected ($P < .001$). While sensitivity was calculated in this study, it was based on MR spectroscopic imaging detection only, and MR imaging information was not incorporated. It has been shown previously that combining MR imaging with MR spectroscopic imaging improves sensitivity and specificity in

prostate tumor detection (9). A full analysis of sensitivity and specificity, including both MR imaging and MR spectroscopic imaging, was beyond the scope of this report.

In lesions with a Gleason score of 7, lesions with a Gleason score of 4 + 3 were found to have *(a)* greater maximum (Cho + Cr)/Cit values than lesions with a Gleason score of 3 + 4 when all lesions were assessed and *(b)* greater mean and maximum metabolite ratios when lesions larger than 5 mm in diameter were tested. This difference was also observed with whole-gland data. Several studies have shown that these two Gleason subscores are used to predict different outcomes in men with clinically localized prostate cancer (35,36). It has also been reported that the difference in outcome in patients with Gleason 3 + 4 cancer versus Gleason 4 + 3 cancer is significant with univariate analysis but not with multivariate analysis when seminal vesicle invasion, extracapsular extension, and lymph node invasion are included (37). Hence, if MR spectroscopic imaging could be used to distinguish Gleason subscores noninvasively, it could be used to aid in pretreatment prognosis, where the previously mentioned pathologic variables are not known.

While there was correlation between MR spectroscopic imaging, metabolite ratio, and tumor grade, there was overlap between ratios for all of the Gleason score groups. In a recent study that used magic-angle spinning nuclear MR of prostate cancer and healthy tissue samples, trends toward an elevated choline and creatine level in patients with cancer were reported; however, there was overlap between low- and high-grade tumor metabolite ratios, and only polyamine/creatine levels were significantly different between low- and high-grade tissues (25). Tissue heterogeneity in these samples was cited as a source of overlap.

While these samples used an average of 8 mg of tissue, MR spectroscopic imaging voxels encompass much larger volumes and would be expected to reflect tissue heterogeneity. It is also possible that volume averaging with normal tissue and voxel bleed due to the point-spread function could contribute to scatter in the ratios, especially in smaller lesions. Polyamine content was not examined in the present study because the spectral resolution did not permit reliable detection of the peak. Another source of scatter in the data results from assigning the noise level to undetectable peaks to calculate a metabolite ratio. This results in, at best, a rough approximation of the metabolite ratio in voxels where Cit is undetectable and could result in substantial scatter in ratio values at the high end of the scale. Absolute quantitation of single peaks on

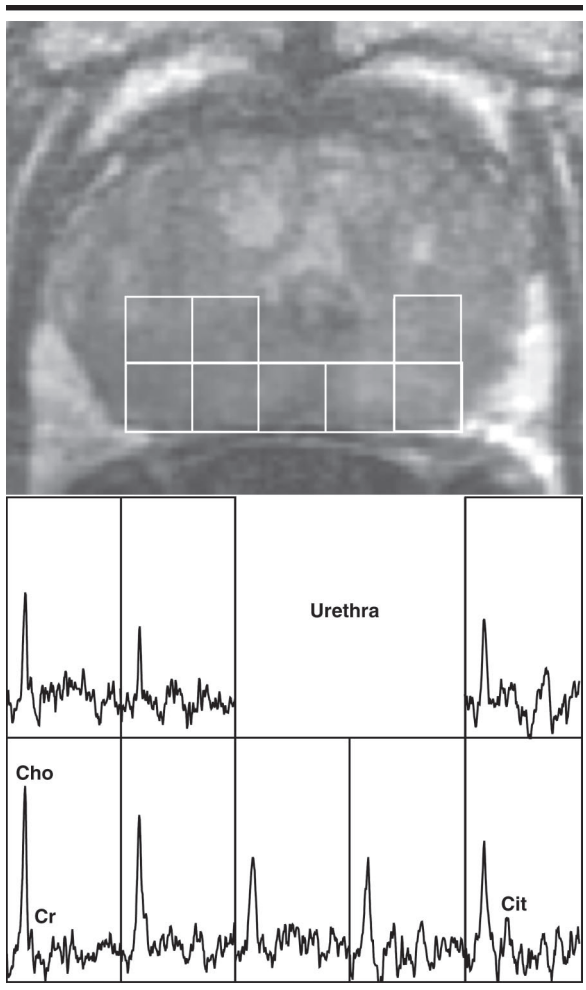

a.

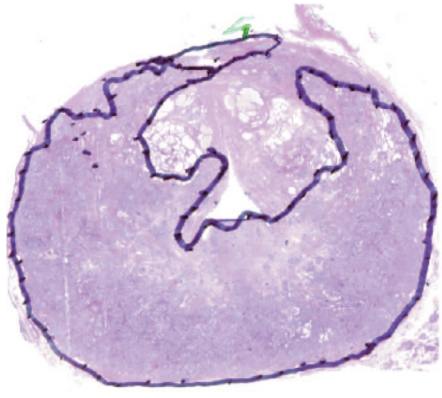

b.

Figure 4. **(a)** Transverse T2-weighted MR image with cancer voxels highlighted and corresponding spectra and **(b)** step-section tumor map obtained in a patient with Gleason 4 + 4 cancer. Areas with a Gleason score greater than or equal to 4 + 4 are outlined. Cho level is elevated in the tumor voxels, and Cit level is low or absent. MR imaging and MR spectroscopy acquisition parameters as the same as those in Figure 2.

TABLE 4
***P* Values for Discriminating between Gleason Scores in Lesions on the Basis of the Mean (Cho + Cr)/Cit Value**

Lesion Gleason Score	Lesion Gleason Score			
	3 + 3	3 + 4	4 + 3	≥4 + 4
3 + 3	NA	.04	<.001	<.001
3 + 4	.04	NA	.07	.015
4 + 3	<.001	.07	NA	.13
≥4 + 4	<.001	.015	.13	NA

Note.—All true-positive lesions were assessed. NA = not applicable.

TABLE 5
***P* Values for Discriminating between Gleason Scores in Lesions on the Basis of the Maximum (Cho + Cr)/Cit Value**

Lesion Gleason Score	Lesion Gleason Score			
	3 + 3	3 + 4	4 + 3	≥4 + 4
3 + 3	NA	.14	<.001	<.001
3 + 4	.14	NA	.003	.001
4 + 3	<.001	.003	NA	.45
4 + 4	<.001	.001	.45	NA

Note.—All true-positive lesions were assessed. NA = not applicable.

TABLE 6
***P* Values Resulting from Test of Hypothesis That Values of Mean (Cho + Cr)/Cit over All True-Positive Lesions in Prostate Gland Differ When Patients Are Stratified by Surgical-Pathologic Gleason Score**

Pathologic Gleason Score	Pathologic Gleason Score			
	3 + 3	3 + 4	4 + 3	≥4 + 4
3 + 3	NA	.304	.003	<.001
3 + 4	.304	NA	.018	.005
4 + 3	.003	.018	NA	.647
4 + 4	<.001	.005	.647	NA

Note.—NA = not applicable.

TABLE 7
***P* Values Resulting from Test of Hypothesis That Values of Maximum Lesion (Cho + Cr)/Cit Averaged over All True-Positive Lesions in Prostate Gland Differ When Patients Are Stratified by Surgical-Pathologic Gleason Score**

Pathologic Gleason Score	Pathologic Gleason Score			
	3 + 3	3 + 4	4 + 3	≥4 + 4
3 + 3	NA	.4002	.001	<.001
3 + 4	.400	NA	.006	.001
4 + 3	.001	.006	NA	.65
4 + 4	<.001	.001	.65	NA

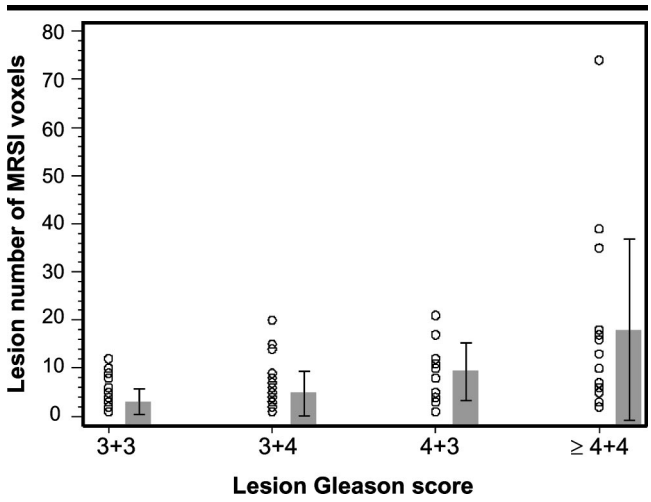

Figure 5. Graph shows number of voxels in lesion detected with MR spectroscopic imaging versus Gleason score of lesion. Number of MR spectroscopic imaging voxels is directly proportional to MR spectroscopic imaging tumor volume (0.12 cm^3 per voxel). Gray columns represent mean value, and error bars represent standard deviation for all lesions with that Gleason score.

the basis of a standard could mitigate this problem but was beyond the scope of the current study.

An interesting, although not unexpected, result in the current study was that tumor volume, as defined by the number of MR spectroscopic imaging–positive voxels, was positively correlated with Gleason score. The largest in-plane diameter at step-section pathologic evaluation also positively correlated with Gleason score. This correlation between tumor volume and grade agrees with several published reports (38,39). The combination of MR spectroscopic imaging metabolite ratio and tumor volume gave the maximum area under the receiver operating characteristic curve. Because the lesion maximum ratio of Cho + Cr to Cit performed as well as or better than the mean value and may be assessed more easily, we recommend that the maximum ratio combined with MR spectroscopic imaging tumor volume be used as an index to help predict tumor aggressiveness.

The current study was limited to peripheral zone lesions for several reasons. In the transition zone, there is substantial overlap in metabolite ratios from tumor and benign tissues, and a clear healthy value versus a tumor cutoff value has not been demonstrated (40). Also, the technology available did not permit the application of oblique saturation bands to limit signal from periprostatic fat. Thus, the rectilinear point-resolved spectroscopy volume was selected to include the entire peripheral zone but not necessarily the entire transition zone if excluding the anterior transition zone could help avoid exciting periprostatic fat. With up to 30% of prostate cancers arising in the transition zone (41), transition zone tumors are not clinically unimportant. Because of the previously mentioned constraints, however, it was deemed best to focus on the peripheral zone.

Another limitation of this study was the exclusion of a number of patients because of technical and clinical issues. Apart from three studies in which hardware failed, the major technical problems, which resulted in the exclusion of 11 reports, were poor signal-to-noise ratio, lipid contamination, and biopsy artifact. A major source of poor signal-to-noise ratio is improper superior-inferior endorectal probe position or rotation of the probe, both of which can happen even when the nurse inserting the probe is highly experienced, especially if the patient is uncomfortable. Lipid contamination resulted mainly from susceptibility effects at the rectal air-tissue interface, which could cause large lipid signals to appear in the spectroscopic imaging data set. The point-resolved spectroscopy volume was chosen to minimize rectal air; however, patient anatomy sometimes required the inclusion of air to excite the entire peripheral zone. Rectal motion due to peristalsis could also degrade the signal-to-noise ratio and exacerbate the lipid contamination problem by altering

the tissue selected with the point-resolved spectroscopy sequence. Finally, despite the fact that the time between biopsy and MR spectroscopic imaging was required to be no less than 6 weeks, some patients still demonstrated substantial biopsy artifact on T1-weighted images and corresponding signal loss at MR spectroscopic imaging, which made the data sets unusable. Chronic prostatitis has been shown to result in an elevated Cho level in the proton spectrum, which mimicks findings associated with cancer (42). Thus, eight patients with pathologically proved chronic prostatitis in the peripheral zone were excluded from the study. For the previously mentioned reasons, 29 of 123 patient data sets were not included in the final analysis. While reducing statistical power, none of these issues was dependent on the Gleason score; therefore, the conclusions are valid.

As mentioned previously, the nonideal point spread function, which arises because of limited k-space sampling, may result in contamination of one voxel with signal from adjacent voxels and some reduction of signal intensity within a voxel. The actual degree of contamination in vivo is difficult to model, however, and depends on the spatial dimensions of structures in the field of view relative to the spatial resolution of the experiment (43). In the present study, effects of most concern were "bleed" of high Cit levels from healthy tissue into adjacent cancerous tissue and, conversely, high Cho levels in tumor bleeding into adjacent healthy tissue. The former effect could reduce the apparent aggressiveness of the cancer, or in the case of small lesions, mask them completely. The latter effect could result in overestimation of cancer volume and/or reduction of the maximum ratios in the cancer. In all CSI studies, the number of k-space points sampled is a compromise between minimizing total imaging time (number of phase encodes) and maximizing signal-to-noise ratio and spatial resolution. The previously mentioned effects may have occurred to some extent and may have contributed to scatter in the data as discussed previously. In the present study, however, the cancer defined with MR spectroscopic imaging usually corresponded closely to the cancer defined with MR imaging, which indicates that gross under- or overestimation of cancer extent and aggressiveness did not occur. In the future, strategies such as optimized k-space sampling (44) or k-space filtering in postprocessing could be implemented to limit point spread function effects.

In conclusion, MR spectroscopic imaging measurements of prostate tumor (Cho + Cr)/Cit and tumor volume correlate with pathologic Gleason score. There is overlap between MR spectroscopic imaging parameters at various Gleason score levels, however, which may reflect both the methodology and physiologic variations. Nonetheless, this study demonstrates that MR spectroscopic imaging has potential in the noninvasive assessment of prostate cancer aggressiveness.

Acknowledgments: The authors thank the investigators at the UCSF Magnetic Resonance Science Center for the use of their data acquisition and processing software.

References

1. Kattan MW, Eastham JA, Stapleton AMF, Wheeler TM, Scardino PT. A preoperative nomogram for disease recurrence following radical prostatectomy for prostate cancer. J Natl Cancer Inst 1998; 90:766–771.
2. Kattan MW, Zelefsky MJ, Kupelian PA, Scardino PT, Fuks Z, Leibel SA. Pretreatment nomogram for predicting the outcome of three-dimensional conformal radiotherapy in prostate cancer. J Clin Oncol 2000; 18:3352–3359.
3. Albertsen PC, Fryback DG, Storer BE, Kolon TF, Fine J. Long-term survival among men with conservatively treated localized prostate cancer. JAMA 1995; 274:626–631.
4. Han M, Partin AW, Zahurak M, Piantadosi S, Epstein JI, Walsh PC. Biochemical (prostate specific antigen) recurrence probability following radical prostatectomy for clinically localized prostate cancer. J Urol 2003; 169:517–523.
5. Partin AW, Piantadosi S, Sanda MG, et al. Selection of men at high risk for disease recurrence for experimental adjuvant therapy following radical prostatectomy. Urology 1995; 45:831–838.
6. Bauer JJ, Connelly RR, Seterhenn IA, et al. Biostatistical modeling using traditional preoperative and pathological prognostic variables in the selection of men at high risk for disease recurrence after radical prostatectomy for prostate cancer. J Urol 1998; 159:929–933.
7. Kattan MW, Wheeler TM, Scardino PT. Postoperative nomogram for disease recurrence after radical prostatectomy for prostate cancer. J Clin Oncol 1999; 17: 1499–1507.
8. Cookson MS, Fleshner NE, Soloway SM, Fair WR. Correlation between Gleason score of needle biopsy and radical prostatectomy specimen: accuracy and clinical implications. J Urol 1997; 157:559–562.
9. Scheidler J, Hricak H, Vigneron DB, et al. Prostate cancer: localization with three-dimensional proton MR spectroscopic imaging—clinicopathologic study. Radiology 1999; 213:473–480.
10. Kurhanewicz J, Vigneron DB, Hricak H, Narayan P, Carroll P, Nelson SJ. Three-dimensional H-1 MR spectroscopic imaging of the in situ human prostate with high (0.24–0.7-cm^3) spatial resolution. Radiology 1996; 198:795–805.
11. Star-Lack J, Nelson SJ, Kurhanewicz J, Huang LR, Vigneron DB. Improved water and lipid suppression for 3D PRESS CSI using RF band selective inversion with gradient dephasing (BASING). Magn Reson Med 1997; 38:311–321.
12. Moyher SE, Vigneron DB, Nelson SJ. Surface coil MR imaging of the human brain with an analytic reception profile correction. J Magn Reson Imaging 1995; 5:139–144.
13. Vigneron DB, Nelson SJ, Moyher S, Kelley D, Kurhanewicz J, Hricak H. An analytical correction of MR images obtained with endorectal or surface coils. J Magn Reson Imaging 1993; 3:142–145.
14. Nelson SJ, Day MR, Carvajal L. Methods for analysis of serial volume MRI and ^1H MRS data for the assessment of response to therapy in patients with brain tumors (abstr). In: Proceedings of the Society of Magnetic Resonance in Medicine and the European Society of Magnetic Resonance in Medicine and Biology. Berkeley, Calif: Society of Magnetic Resonance in Medicine, 1995; 1960.
15. Bottomley P. Selective volume method for performing localized NMR spectroscopy. USA patent 4, 1984; 480:228.
16. Brown TR, Kincaid BM, Ugurbil K. NMR chemical shift imaging in three dimensions. Proc Natl Acad Sci U S A 1982; 79:3523–3526.
17. Males R, Vigneron D, Star-Lack J, et al. Clinical application of BASING and spectral/spatial water and lipid suppression pulses for prostate cancer staging and localization by in vivo 3D 1H magnetic resonance spectroscopic imaging. Magn Reson Med 2000; 43:17–22.
18. Liang KY, Zeger SL. Longitudinal data analysis using generalized linear models. Biometrics 1986; 73:13–22.
19. Wefer AE, Hricak H, Vigneron DB, et al. Sextant localization of prostate cancer: comparison of sextant biopsy, magnetic resonance imaging and magnetic resonance spectroscopic imaging with step section histology. J Urol 2000; 164:400–404.
20. Steinberg DM, Sauvageot J, Piantadosi S, Epstein JI. Correlation of prostate needle biopsy and radical prostatectomy Gleason grade in academic and community settings. Am J Surg Pathol 1997; 21:566–576.
21. Males R, Vigneron D, Nelson S, et al. Addition of MR spectroscopic imaging to MRI significantly improves detection and localization of prostate cancer (abstr). In: Proceedings of the Sixth Meeting of the International Society for Magnetic Resonance in Medicine. Berkeley, Calif: International Society for Magnetic Resonance in Medicine, 1998; 487.
22. Vigneron DB, Males R, Noworolski S, et al. 3D MRSI of prostate cancer: correlation with histologic grade (abstr). In: Proceedings of the Sixth Meeting of the International Society for Magnetic Resonance in Medicine. Berkeley, Calif: International Society for Magnetic Resonance in Medicine, 1998; 488.
23. Zakian KL, Sircar K, Kleinman S, Shukla-Dave A, Kattan MW, Hricak H. Correlation of proton MR spectroscopic imaging

with Gleason score based on step section radical prostatectomy (abstr). Radiology 2002; 225(P):1525.
24. Gleason DF, Group VACU. Histologic grading and clinical staging of prostatic carcinoma. In: Tannebaum M, ed. Urologic pathology: the prostate. Philadelphia, Pa: Lea & Febiger, 1977; 171–197.
25. Swanson MG, Vigneron DB, Tabatabai ZL, et al. Proton HR-MAS spectroscopy and quantitative pathologic analysis of MR imaging and 3D-MRSI-targeted postsurgical prostate tissues. Magn Reson Med 2003; 50:944–954.
26. Fulham MJ, Bizzi A, Dietz MJ, et al. Mapping of brain tumor metabolites with proton MR spectroscopic imaging: clinical relevance. Radiology 1992; 185:675–686.
27. McBride DQ, Miller BL, Nikas DL, et al. Analysis of brain tumors using ^{1}H magnetic resonance spectroscopy. Surg Neurol 1995; 44:137–144.
28. Heesters MA, Kamman RL, Mooyaart EL, Go KG. Localized proton spectroscopy of inoperable brain gliomas: response to radiation therapy. J Neurooncol 1993; 17: 27–35.
29. Sijens PE, Knopp MV, Brunetti A, et al. ^{1}H MR spectroscopy in patients with metastatic brain tumors: a multicenter study. Magn Reson Med 1995; 33:818–826.
30. Rutter A, Hugenholtz H, Saunders JK, Smith ICP. One-dimensional phosphorus-31 chemical shift imaging of human brain tumors. Invest Radiol 1995; 30: 359–366.
31. Koutcher JA, Ballon D, Graham M, et al. P-31 NMR spectra of extremity sarcoma: diversity of metabolic profiles and changes in response to chemotherapy. Magn Reson Med 1990; 16:19–34.
32. Dewhirst MW, Sostman HD, Leopold KA, et al. Soft-tissue sarcomas: MR imaging and MR spectroscopy for prognosis and therapy monitoring: work in progress. Radiology 1990; 174:847–853.
33. Smith TA, Eccles S, Ormerod MG, Tombs AJ, Titley JC, Leach MO. The phosphocholine and glycerophosphocholine content of an oestrogen-sensitive rat mammary tumour correlates strongly with growth rate. Br J Cancer 1991; 64:821–826.
34. Aboagye EO, Bhujwalla ZM. Malignant transformation alters membrane choline phospholipid metabolism of human mammary epithelial cells. Cancer Res 1999; 59:80–84.
35. Sakr WA, Tefilli MV, Grignon DJ, et al. Gleason score 7 prostate cancer: a heterogeneous entity? correlation with pathologic parameters and disease-free survival. Urology 2000; 56:730–734.
36. Han M, Snow PB, Epstein JI, et al. A neural network predicts progression for men with Gleason score 3 + 4 versus 4 + 3 tumors after radical prostatectomy. Urology 2000; 56:994–999.
37. Herman CM, Kattan MW, Ohori M, Scardino PT, Wheeler TM. Primary Gleason pattern as a predictor of disease progression in Gleason score 7 prostate cancer: a multivariate analysis of 823 men treated with radical prostatectomy. Am J Surg Pathol 2001; 25:657–660.
38. Eichelberger LE, Koch MO, Daggy JK, Ulbright TM, Eble JN, Cheng L. Predicting tumor volume in radical prostatectomy specimens from patients with prostate cancer. Am J Clin Pathol 2003; 120:386–391.
39. Augustin H, Hammerer PG, Graefen M, et al. Characterisation of biomolecular profiles in primary high-grade prostate cancer treated by radical prostatectomy. J Cancer Res Clin Oncol 2003; 129:662–668.
40. Zakian KL, Eberhardt S, Hricak H, et al. Transition zone prostate cancer: metabolic characteristics at 1H MR spectroscopic imaging—initial results. Radiology 2003; 229:241–247.
41. McNeal JE, Redwine EA, Freiha FS, Stamey TA. Zonal distribution of prostatic adenocarcinoma: correlation with histologic pattern and direction of spread. Am J Surg Pathol 1988; 12:897–906.
42. Shukla-Dave A, Koutcher JA, Eberhardt S, et al. 1H MRSI findings in prostatitis (abstr). In: Proceedings of the Eleventh Meeting of the International Society for Magnetic Resonance in Medicine. Berkeley, Calif: International Society for Magnetic Resonance in Medicine, 2003; 1291.
43. Murphy-Boesch J, Jiang H, Stoyanova R, Brown TR. Quantification of phosphorus metabolites from chemical shift imaging spectra with corrections for point spread effects and B1 inhomogeneity. Magn Reson Med 1998; 39:429–438.
44. Hugg JW, Maudsley AA, Weiner MW, Matson GB. Comparison of k-space sampling schemes for multidimensional MR spectroscopic imaging. Magn Reson Med 1996; 36:469–473.